Cytoplasmic cAMP-sensing domain of hyperpolarization-activated cation (HCN) channels uses two structurally distinct mechanisms to regulate voltage gating

Nadine L. Wicks[a], Tammy Wong[b], Jinyi Sun[b], Zarina Madden[b], and Edgar C. Young[b,1]

[a]Department of Molecular Pharmacology, Physiology and Biotechnology, Brown University, Providence, RI 02912; and [b]Department of Molecular Biology and Biochemistry, Simon Fraser University, Burnaby, BC, Canada V5A 1S6

Edited by Richard W. Aldrich, University of Texas at Austin, Austin, TX, and approved December 2, 2010 (received for review August 26, 2010)

Voltage gating of hyperpolarization-activated cation (HCN) channels is potentiated by direct binding of cAMP to a cytoplasmic cAMP-sensing domain (CSD). When unliganded, the CSD inhibits hyperpolarization-dependent opening of the HCN channel gate; cAMP binding relieves this autoinhibition so that opening becomes more favorable thermodynamically. This autoinhibition-relief mechanism is conserved with that of several other cyclic nucleotide receptors using the same ligand-binding fold. Besides its thermodynamic effect, cAMP also modulates the depolarization-dependent deactivation rate by kinetically trapping channels in an open state. Here we report studies of strong open-state trapping in an HCN channel showing that the well-established autoinhibition-relief model is insufficient. Whereas deletion of the CSD mimics the thermodynamic open-state stabilization usually associated with cAMP binding, CSD deletion removes rather than mimics the kinetic effect of strong open-state trapping. Substitution of different CSD sequences leads to variation of the degree of open-state trapping in the liganded channel but not in the unliganded channel. CSD-dependent open-state trapping is observed during a voltage-dependent deactivation pathway, specific to the secondary open state that is formed by mode shift after prolonged hyperpolarization activation. This hysteretic activation–deactivation cycle is preserved by CSD substitution, but the change in deactivation kinetics of the liganded channel resulting from CSD substitution is not correlated with the change in autoinhibition properties. Thus the liganded and the unliganded forms of the CSD respectively provide the structural determinants for open-state trapping and autoinhibition, such that two distinct mechanisms for cAMP regulation can operate in one receptor.

allosteric | ligand gating | pacemaker channel | patch clamp

The second messenger cAMP targets multiple receptors employing a conserved 120-residue cAMP-binding fold (reviewed in ref. 1). Some cAMP receptors are soluble proteins such as protein kinase A (PKA) or the G-protein exchange factor, EPAC, but others are ion channels such as the hyperpolarization-activated cation (HCN) channels from the brain and heart (reviewed in ref. 2). Understanding how cAMP regulates HCN channels is important because gene transfer of engineered HCN channels has shown promise for treating sick-sinus syndrome (3). Unlike the soluble receptors, HCN channels have an efficient mechanism for activation without cAMP, through hyperpolarization of the membrane potential. Thus it is unclear if mechanistic features of cAMP transduction in HCN channels are an exact parallel of those in soluble receptors, or if HCN channels might have evolved unique functions for the cAMP-binding fold in the unusual context of a voltage-sensing transmembrane receptor.

HCN channels are tetramers of homologous subunits; each subunit has six membrane-spanning helices (S1–S6) homologous to those of voltage-gated potassium channels, with a voltage-sensing domain in S1–S4 (4). Hyperpolarization drives inward movement of the positively charged S4 (5), which is coupled to opening of the pore gate formed by the cytoplasmic C-terminal ends of the four S6 helices in the tetramer (6). S6 in each subunit is followed by an 80-residue "C-linker" with an unusual multihelix fold (7), then the cAMP-binding fold and a poorly conserved "extreme C-terminal" region. The C-linker and cAMP-binding fold together can be viewed as one "cAMP-sensing domain" (CSD; see Fig. 1*A*, *Top*), based on domain stability (7) and the C-linker's functional importance (8).

Cyclic AMP binding potentiates hyperpolarization-dependent activation of HCN channels (9). That is, cAMP increases thermodynamic stability of the open channel relative to the closed channel, so that the voltage needed for half-maximal activation ($V_{1/2}$) becomes less negative. A similar $V_{1/2}$ shift can be produced by deleting the CSD through enzymatic or genetic truncation (10, 11). This establishes a classical autoinhibition mechanism (12) as the basis for cAMP regulation of HCN channels, in analogy with PKA (13) and EPAC (14). Thus the unliganded ("apo") CSD inhibits an intrinsic activity of the channel, and the liganded ("holo") form of the CSD has weakened or nonexistent capability for this inhibition, so that cAMP binding mimics CSD deletion. Because the autoinhibition-relief model attributes specific regulatory function to the apo CSD rather than the holo CSD, we introduce the designation "apo-driven" for this mechanism type. In a "holo-driven" mechanism, by contrast, the presence of the CSD with bound ligand would be required for a particular HCN channel structure that achieves optimal activation. A holo-driven mechanism has been proposed for the dimeric *Escherichia coli* catabolite activator protein: The two liganded cAMP-binding folds form a scaffold to hold the two DNA-binding domains in the correct relative orientation for binding successive DNA major grooves (15).

Besides its thermodynamic effect ($V_{1/2}$ shift), cAMP also affects kinetic features of HCN channel gating: It speeds up activation and slows down deactivation. These effects are in keeping with autoinhibition relief—cAMP binding favors the open state—but in principle cAMP's thermodynamic and kinetic effects might not arise from the same structural mechanism. We previously found a transmembrane domain mutation that enhanced cAMP's effect on deactivation rate but did not greatly alter $V_{1/2}$ values with or without cAMP (16). Slowing of deactivation implies strengthening a kinetic trap for the open state, and it is unclear how this trapping mechanism is related to autoinhibition relief. Here we show that the strong open-state trapping induced by cAMP strictly

Author contributions: N.L.W. and E.C.Y. designed research; N.L.W., T.W., J.S., Z.M., and E.C.Y. performed research; J. S. and Z. M. constructed chimeras; N.L.W., T.W., J.S., and E.C.Y. collected and analyzed electrophysiological data; and N.L.W. and E.C.Y. wrote the paper.

The authors declare no conflict of interest.

This article is a PNAS Direct Submission.

[1]To whom correspondence may be addressed at: Department of Molecular Biology and Biochemistry, Simon Fraser University, 8888 University Drive, Burnaby, BC, Canada V5A 1S6. E-mail: youngec@sfu.ca.

This article contains supporting information online at www.pnas.org/lookup/suppl/doi:10.1073/pnas.1012750108/-/DCSupplemental.

requires an intact and liganded CSD, unlike autoinhibition relief. Further, the potency of kinetic trapping in a liganded channel can be modulated by substitution of CSDs derived from different HCN channel subtypes, but the extent of trapping does not correlate with the extent of autoinhibition. Thus cAMP regulates HCN channel gating through at least two structurally distinct mechanisms.

Results and Discussion

Rationale. The autoinhibition model for HCN channels is apo-driven: It postulates inhibitory action of the unliganded apo form of the CSD. This implicitly assumes that the transmembrane domain S1–S6 has intrinsic "default" gating properties that are unmasked when the CSD is deleted or when the CSD is disabled by cAMP binding (the liganded holo form) (11). We explored how open-state trapping during deactivation might change upon modifying the CSD sequence or removing it entirely.

We constructed a series of chimeric HCN channel derivatives (Fig. 1*A*, *Bottom*) with CSD sequences derived from mouse HCN1, HCN2, and HCN4, keeping non-CSD sequence invariant so that functional differences could be attributed to CSD sequence differences. We also studied a truncated construct (C-del) missing the entire CSD. To facilitate study of open-state trapping, all constructs used the transmembrane domain of mouse HCN4 with a previously characterized mutation, K381E, that enhances open-state trapping by holo HCN4 channels (16). The K381E mutation produces an "ultrasustained activation" phenotype whose defining feature is that deactivation at weakly depolarized voltages is very slow, requiring tens of seconds for complete closing. The ultrasustained activation phenotype appears only for the holo form (with saturating cAMP at 10 μM or greater), and this helps to distinguish the deactivation kinetics of holo vs. apo channels. At the same time, the K381E mutation does not produce large changes in $V_{1/2}$ or Boltzmann g-V slope, and it preserves the cAMP-dependent $V_{1/2}$ shift observed in HCN4.

As in our previous study (16), our constructs omitted the extreme C-terminal region and used the cytoplasmic N-terminal region from mouse HCN2 to facilitate heterologous expression (17). Each construct was expressed as homomers in *Xenopus* oocytes and showed activation behavior typical of HCN channels when tested by voltage clamp of inside-out excised macropatches. After activation by step hyperpolarization, sigmoidal deactivation time courses ("tail" currents) were obtained by depolarizing the membrane back to the holding voltage of −40 mV. The tail currents (Fig. 1 *B* and *D*) were well-described by a single-exponential decay with time constant τ_{deact} after omission of an initial delay (18) of duration d (defined by an iterative curve-fitting method in ref. 16).

The CSD Is Necessary for Open-State Trapping of Liganded Channels. We compared chimera C-del, lacking the CSD, to the previously characterized chimera C-2 (16); the latter has the CSD from HCN2, which can support strong cAMP regulation (11, 19) and the ultrasustained activation phenotype of K381E with strong open-state trapping (16). C-del is inhibition-free as expected, because its $V_{1/2}$ (−98.9 ± 1.7 mV, $n = 5$) is considerably depolarized from that of apo C-2 (−128.1 ± 7.9 mV, $n = 4$; see Fig. 1 *B* and *C* and Table S1). The autoinhibition-relief model then predicts that deactivation kinetics of C-del should resemble those of holo C-2 whose inhibition is relieved. But surprisingly to the contrary, deactivation of C-del is very fast (τ_{deact} = 820 ± 440 ms, $n = 8$) compared to holo C-2, which deactivates very slowly ($\tau_{deact,\ cA}$ = 6,200 ± 2,700 ms, $n = 4$). Although it is known that HCN channels form multiple open states with increasing stability (16, 20), the 3 s of activation at −140 mV is quite sufficient for C-del to reach the terminal state in its activation pathway: Hyperpolarizations from −130 mV to −160 mV produced indistinguishable deactivation traces with fast kinetics (Fig. 1*B*, gray trace). Thus, although the autoinhibition-relief model can explain thermodynamic $V_{1/2}$ shift effects of cAMP, it is insufficient to predict deactivation kinetics of holo C-2 channels. The default gating properties revealed by C-del are not only "inhibition-free" but also "trap-free." Then some additional mechanism in holo C-2 channels produces very strong open-state trapping, employing structural elements within the liganded CSD—a holo-driven mechanism for kinetic stabilization of the open state.

Because the autoinhibitory apo CSD thermodynamically destabilizes the open state relative to the closed state, an associated kinetic effect might be expected for any processes whose rate-

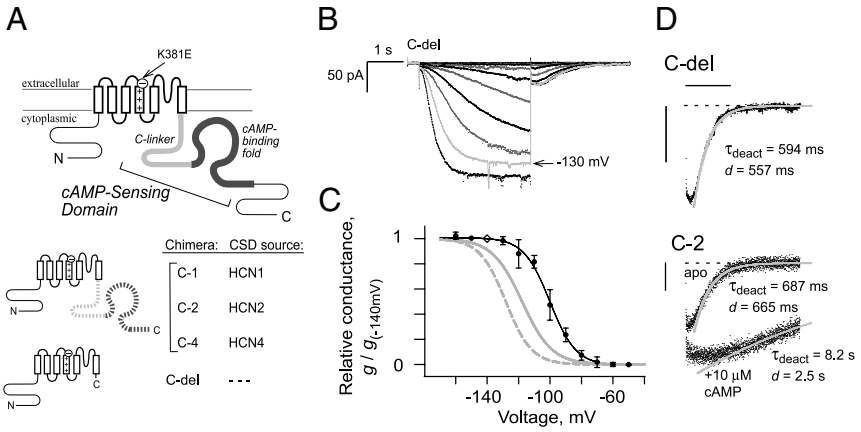

Fig. 1. Strong open-state trapping of liganded (holo) HCN channels is abolished by deletion of the CSD. (*A*) Topology of HCN channel subunit, with composition of CSD-substitution derivatives. Externally facing K381E mutation enables cAMP-dependent ultrasustained activation phenotype in C-2 (16). (*B*) Macroscopic currents from inside-out excised patches containing homomeric channels of C-del without cAMP. From a resting voltage of −40 mV, 3-s hyperpolarization pulses were applied in 10-mV intervals starting at −50 mV. Sweep with −130 mV activation (light gray trace) has a deactivation tail current coincident with that obtained from −140 mV activation. (*C*) Summary conductance–voltage (g-V) relationship of C-del (protocol as in *B*). Points plot means of leak-subtracted conductances, measured directly after 3-s activation and normalized to the value from −140 mV activation (diamond) in the same patch. Error bars show SD; $n = 3$ to 7 patches for each point. Black solid curve shows Boltzmann equation fit (see *Materials and Methods*) to C-del data with parameters (in mV, ±SEM) as follows: $V_{1/2} = -100.1 \pm 0.7$, $s = 8.3 \pm 0.6$. Gray curves are g-V relations for C-2 homomers with parameters (±SEM, in mV) taken from ref. 16: apo C-2 (dashed gray), $V_{1/2} = -128.1 \pm 0.3$, $s = 8.2 \pm 0.3$; holo C-2 (solid gray, saturating 10 μM cAMP), $V_{1/2} = -117.7 \pm 0.5$, $s = 9.5 \pm 0.4$. (*D*) Deactivation tail currents (data points) at −40 mV (after 3-s activation at −140 mV) of C-del homomers without cAMP (*Top*), and C-2 homomers (*Bottom*) in apo and holo form. Dashed line marks zero current level. Gray curves are single-exponential fits to time courses with omission of initial delay d (see *Materials and Methods*), but are extrapolated back to show lack of fit during the delay. Scale bars: horizontal, 2 s; vertical, 20 pA.

limiting step is sensitive to the inhibition. For instance, apo C-2 exhibits slower activation kinetics than the inhibition-free C-del ($\tau_{act,apo}$ values in Table S1). If we suppose that autoinhibition relief is the *sole* mechanism for cAMP effects, then autoinhibition should make apo C-2 deactivate faster than C-del, in the same way that removing cAMP from any HCN channel speeds up deactivation. To test this prediction, we compared C-del deactivation to apo C-2 deactivation (Fig. 1*D*, *Bottom*, apo); the activation voltage of −140 mV was not saturating for apo C-2 channels (16) but was chosen to match the saturating stimulus applied to C-del. Apo C-2 deactivation kinetics ($\tau_{deact,apo} = 720 \pm 430$ ms, $n = 7$) are in fact not significantly different from those of C-del ($P > 0.6$). In fact, this similarity in $\tau_{deact,apo}$ values holds for all our chimeras in apo form (Fig. 2*A*, *Left*, open points; no significant differences by ANOVA, $P > 0.4$).

One explanation for the similar $\tau_{deact,apo}$ values could be that the secondary mechanism does operate to kinetically stabilize the open state in apo C-2, but is coincidentally counteracted by a destabilizing factor from the autoinhibition mechanism so that overall deactivation kinetics are like C-del. However, repeating this coincidence to produce similar $\tau_{deact,apo}$ for all our chimeras is improbable, because the chimeras show very different $V_{1/2}$ in apo form (Fig. 2*A*, *Right*, open points) indicating different extents of autoinhibition. We favor the simpler interpretation that the apo CSD does not influence the rate-limiting step of deactivation at all; the apo-driven autoinhibition mechanism influences only the activation pathway and not the deactivation pathway [known to be different from the reverse of the activation pathway (20, 21)].

Strength of Open-State Trapping Varies with CSD Sequence for Holo Channels. Extensive study of C-del was difficult because of inefficient expression (success in <20% of patches), but chimeras C-1 and C-4 expressed more reliably and enabled additional tests of the autoinhibition-relief model, independent of C-del experiments (Fig. 2). This was possible because C-1 could not support the ultrasustained activation phenotype of C-2. Deactivation of holo C-1 ($\tau_{deact,cA} = 1{,}920 \pm 880$ ms, $n = 9$) is significantly faster than holo C-2 ($P < 0.001$). This functional difference does not reflect lack of cAMP binding in C-1, because removal of cAMP from C-1 does hyperpolarize $V_{1/2}$, speed up deactivation, and slow down activation as expected for the restoration of autoinhibition (Fig. 2*B*, *Top*; see $\Delta V_{1/2}$, $\tau_{deact,cA}/\tau_{deact,apo}$, and $\tau_{act,cA}/\tau_{act,apo}$ in Table S1). In contrast, holo C-4 shows slow deactivation like C-2 (Fig. 2*B*, *Bottom*), confirming our previous finding (16) that the holo CSD of either HCN2 or HCN4 can support very strong open-state trapping.

If autoinhibition relief is solely responsible for cAMP effects, then the faster deactivation of holo C-1 (compared to holo C-2 or C-4) can be explained only by postulating that holo C-1 retains a greater degree of residual autoinhibition than holo C-2 or C-4. This postulate leads to the prediction that C-1 should also exhibit the most negative $V_{1/2}$ of the CSD-replacement chimeras when tested in holo form. In fact, the opposite relationship is true (Table S1): Holo C-1 has a significantly more positive $V_{1/2}$ than holo C-2 ($P < 0.006$). These findings show again that the autoinhibition-relief model is insufficient to explain the determinants of deactivation kinetics in our chimeras. Besides any residual inhibition from the liganded CSD, there must exist a structurally distinct secondary mechanism that makes open-state trapping stronger in holo C-2 than in holo C-1. The quantitative contribution of this secondary mechanism to other gating properties like $V_{1/2}$, and which residues in the C-linker or cAMP-binding fold of C-2 are essential for strong trapping, remain undetermined at this time.

Open-state trapping in liganded channels is thus malleable with a strength that depends on the CSD sequence, and we previously showed that its strength also changes according to mutation of K381 (16). Thus the CSD and transmembrane domain work together to control cAMP-dependent deactivation kinetics, as previously noted for control of cAMP-dependent $V_{1/2}$ shift (11, 19). Without the K381E mutation, the quantitative effects of CSD replacement may or may not be the same as seen here; this caveat applies to any comparison of substitution chimeras using a single invariant background sequence, which can never capture the diversity of sequences from native HCN channel subtypes. Our non-CSD sequence was chosen for the experimental convenience of slower deactivation kinetics, because our intent is not to replicate the quantitative kinetics of any particular native

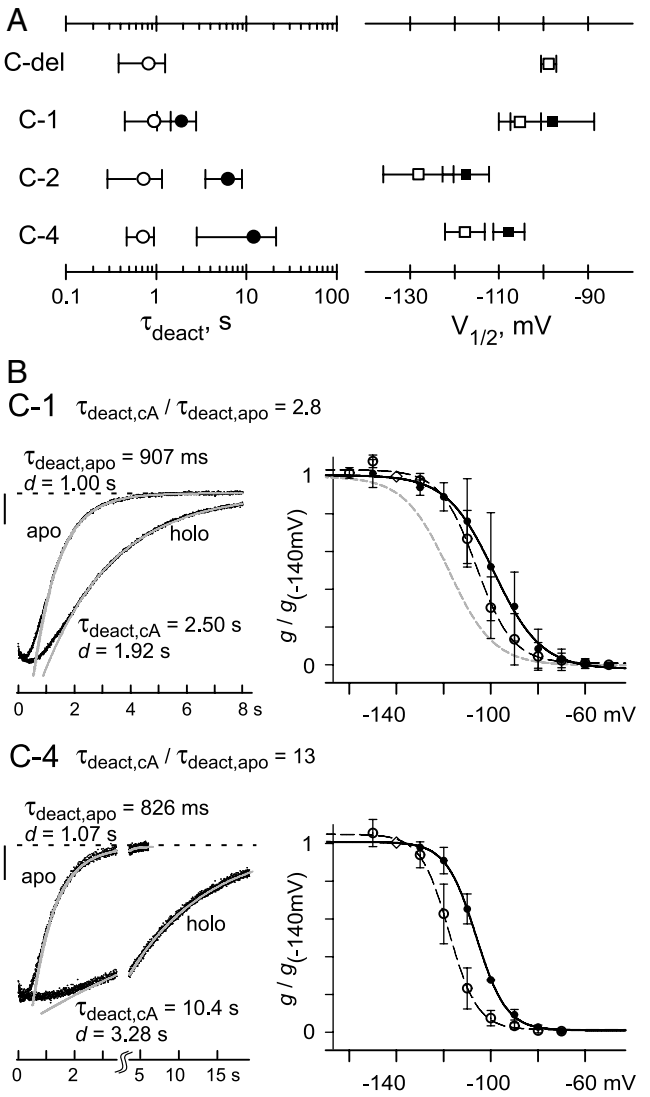

Fig. 2. Open-state trapping in holo channels is sensitive to changes in CSD sequence. (*A*) Points plot mean ± SD ($n = 3$ to 16 for each point) of τ_{deact} and $V_{1/2}$ for homomeric channels in apo (open) or holo form (solid); detailed values and conditions are given in Table S1. (*B*) Deactivation tail currents (*Left*) and summary *g*-V relations (*Right*) for C-1 (*Top*) and C-4 (*Bottom*). Tail currents were measured as in Fig. 1*D* at −40 mV after activation for 3 s at −140 mV (C-1) or 5 s at −130 mV (C-4). Vertical scale bar: 20 pA; long time scale after axis break accommodates slow deactivation of C-4. The *g*-V relations were collected and normalized as in Fig. 1*C*; for C-4, conductances were measured after 5-s activation pulses. Apo: open points (data) and black dashed curves (fits); holo: solid points (data) and black solid curves (fits). Boltzmann parameters (±SEM, in mV): apo C-1, $V_{1/2} = -106.1 \pm 0.6$, $s = 7.7 \pm 0.6$; holo C-1, $V_{1/2} = -98.7 \pm 0.7$, $s = 10.0 \pm 0.6$; apo C-4, $V_{1/2} = -117.7 \pm 0.3$, $s = 6.0 \pm 0.3$; holo C-4, $V_{1/2} = -106.3 \pm 0.2$, $s = 6.4 \pm 0.2$. Gray dashed curve in the C-1 *g*-V graph (*Top*) shows *g*-V relation for apo C-2 from Fig. 1*C*.

subtype. The significance of our findings is to show that structural differences between various holo CSDs can be detected by examining deactivation kinetics and that a holo-driven mechanism in the CSD is required to explain the observed effects.

Weakened Open-State Trapping in C-1 Does not Indicate an Altered Activation–Deactivation Cycle. The weak trapping of C-1 raises the possibility that C-1 uses mechanistic steps qualitatively different than those of C-2 and C-4. To test similarity in deactivation pathways of C-1 and C-2, we examined key mechanistic properties that rely on the transmembrane domain rather than the CSD.

A mechanistic hallmark of the HCN channel reaction pathway is an "activation mode shift" imparting hysteresis to the activation–deactivation cycle (Fig. 3*A*): After a hyperpolarization, multiple consecutive open states are formed with different conformations in the voltage-sensing domain (20–22). In K381E channels, we previously found that the initial open state (O_I) exhibits generally faster deactivation kinetics than the terminal open state (O_{II}), and O_I cannot support the ultrasustained activation phenotype (16). Thus the weak open-state trapping of C-1 might reflect an arrest of mode shift, keeping channels in O_I. We excluded this by isolating O_I, applying hyperpolarizations too brief for completion of mode shift (16, 20). Holo C-1 deactivation traces after 50-ms activation show O_I channels as a fast phase decaying within a few hundred milliseconds ("fast" in Fig. 3*B*); O_{II} channels are seen as a slow phase whose time constant τ_{slow} matches that seen after conventional 3-s hyperpolarization (gray curves in Fig. 3*B*; cf. Fig. 2*B*, *Top Left*; see Fig. S1 for extraction of τ_{slow}). The slow phase's amplitude made up less than 50% of the total decay in all recordings using 50-ms activation; this confirms the fast and slow phases represent subpopulations of open states with independent deactivation pathways, and not a single open state deactivating by consecutive fast and slow steps before closure (in which case the slow step would dominate kinetics). Thus activation of holo C-1 does initially form a short-lived O_I subpopulation and then progresses normally through mode shift to reach O_{II}, like other HCN channels including C-2 (comparison in Fig. S1*D*).

Voltage-dependence reflecting S4 movement (23) is another mechanistic hallmark of HCN channel deactivation that is exhibited by O_{II} deactivation of C-1. We quantified the effects of a 20-mV shift in the holding voltage used to measure deactivation (Fig. S2*A*) under both weak and strong depolarization regimes. In the weak depolarization regime, a shift from −60 mV to −40 mV sped up the deactivation time constant of holo C-1 by a factor of 2.1 ± 0.2 ($n = 3$); in the strong depolarization regime, a shift from +40 mV to +60 mV sped up deactivation by a factor of only 1.5 ± 0.1 ($n = 4$). The attenuation of the voltage-dependence factor with stronger depolarization agrees with previous observations of a change in rate-limiting step (24): As S4 movement becomes progressively faster, deactivation kinetics become dominated by a step with lesser or no voltage dependence, attributed to gate closure (25). More important, voltage-dependence factors for holo C-1 in either depolarization regime were not significantly different from corresponding voltage-dependence factors for holo C-2 (Fig. 4, $P > 0.1$). The match supports the notion that during holo O_{II} deactivation, the conformational changes of the transmembrane domain are mechanistically similar in C-1 and C-2, with differences confined to the quantitative rates (Fig. S2*B* shows a similar match for apo channels).

Taken in all, C-1 and C-2 both use reaction pathways typical of HCN channels, both for the activation mode shift forming O_{II} and for voltage-dependent deactivation removing O_{II}. But the detailed structure of the cAMP-liganded O_{II} state is not the same in these two channels, producing a dramatically longer lifetime for the O_{II} of holo C-2.

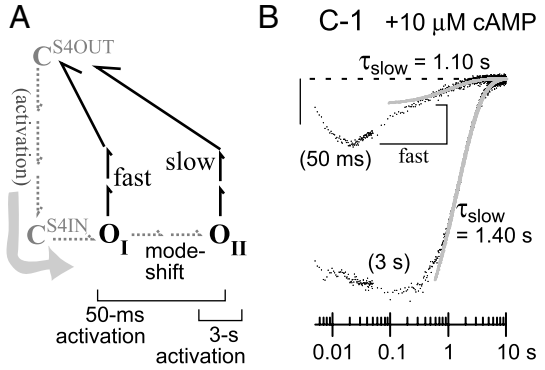

Fig. 3. C-1 channels undergo activation mode shift typical of HCN channels. (*A*) Deactivation pathways of open states (O_I, O_{II}) in a simplified model (16); only apo states are shown, omitting the parallel tier of holo states. Brackets show open states populated after activating pulses of 50 ms or 3 s. Each open state has a multistep deactivation pathway dominated by one rate-limiting step, and thus decays with a single exponential following a delay. (*B*) Deactivation tail currents of holo C-1 at −40 mV after activating for 50 ms at −215 mV or 3 s at −140 mV. Time axis is logarithmic to accommodate the capacitance transient (initial 20 ms), the subpopulation of rapidly closing channels ("fast," visible only after 50-ms activation) and the slowly decaying O_{II} subpopulation (gray curves from multiexponential fitting; Fig. S1 shows detailed fitting and similar data for apo C-1). Vertical scale bar: 20 pA. Data points are undersampled (100 Hz; 2 kHz in initial 50 ms) for clearer printing.

Implications of a Second cAMP-Regulation Mechanism. A possible mechanistic interpretation for the two cAMP-regulation mechanisms of C-2 is shown in Fig. 5. It uses a simplifying assumption, consistent with our findings, that the apo-driven mechanism of autoinhibition primarily influences the activation pathway, whereas the holo-driven mechanism of open-state trapping primarily influences the deactivation pathway. In apo channels, the CSD affects equilibria between channel states up to the formation of O_{II}, with a mechanism believed to involve intersubunit interactions in the tetrameric channel (26), but it has little effect on the subsequent steps used for O_{II} deactivation. Conversely in holo channels, some highly stable structure creates a high kinetic barrier for a voltage-dependent step in the O_{II} deactivation pathway, possibly through CSD interactions with the S4-S5 linker (27, 28), but this does not apply to deactivation from the preceding O_I state (16). The assignment of autoinhibition and open-state trapping mechanisms to separate legs of the activation–deactivation cycle implies that when functional properties of HCN channels are described, the effect of saturating cAMP on deactivation rate (the τ_{deact} ratio, $\tau_{deact,cA}/\tau_{deact,apo}$) and on voltage activation ($V_{1/2}$ shift) should both be reported, providing distinct measures of cAMP efficacy reflecting different mechanistic roles of the CSD. The τ_{deact} ratio should be measured

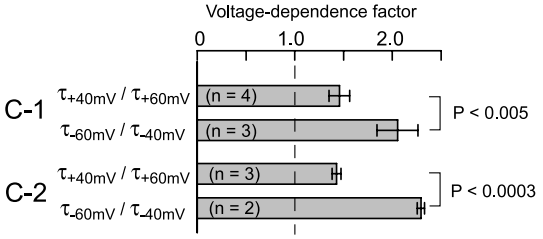

Fig. 4. O_{II} deactivation in C-1 channels is voltage-dependent. Holo O_{II} states were formed (activation for 3 s at −140 mV or 2 s at −160 mV for C-1, and for 2 s at −160 mV for C-2), and deactivation time constants were measured at various holding voltages (subscript on τ symbol). Ratios of time constants from specified pairs of holding voltages provide voltage-dependence factors. Bars plot voltage-dependence factors (mean ± SD) and brackets with *t* test *P* values mark comparisons showing significant difference, showing attenuation of voltage dependence at positive voltages. See Fig. S2 for examples of holo C-1 current traces, and compiled data for apo C-1 and C-2.

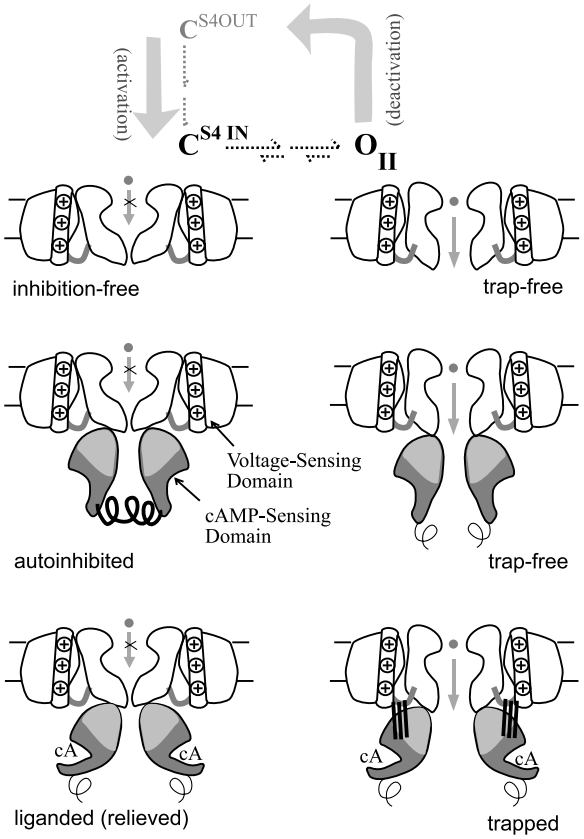

Fig. 5. Two mechanisms for cAMP regulation. Schematic shows proposed structural features in selected channel states formed after hyperpolarization during the activation pathway. Autoinhibitory element (coiled spring) in the apo CSD stabilizes the closed state (C^{S4IN}), but is removed by either cAMP binding or CSD deletion. After gate opening and mode shift to form O_{II}, the apo CSD's autoinhibitory features do not influence deactivation kinetics (broken spring). Mode shift uniquely enables the holo CSD to form a highly stable structure (ligatures to transmembrane domain) resulting in open-state trapping during deactivation.

at a weakly depolarized voltage where S4 movement is rate-limiting. The quantitative effect of cAMP on activation kinetics (e.g., $\tau_{act,cA}/\tau_{act,apo}$ in Table S1) similarly depends on which step is rate-limiting but, like $V_{1/2}$, it primarily reflects autoinhibition.

Various cAMP receptors employ the conserved cAMP-binding fold, but conservation of their mechanistic features is not fully understood (29, 30). PKA sets the classic example of autoinhibition in a cAMP receptor, but HCN channels differ from PKA in key respects. Whereas PKA catalyses a metabolic modification (phosphorylation), HCN channels produce a time-resolved electrical response in rhythmically firing cells (20, 31). Oscillatory properties are sensitive to channel kinetics just as much as to channel thermodynamics, so fine-tuned control of HCN channel kinetics could have an adaptive benefit in evolution. In PKA, holo-driven mechanisms are unavailable because cAMP activation entails dissociation of the catalytic subunit from its autoinhibitory regulatory subunit, and PKA has no alternative deactivation pathway in the presence of cAMP. In contrast, HCN channels have their CSD permanently fused to their catalytic region (the pore), and depolarization-dependent deactivation can occur with or without cAMP bound. These structural and functional features provide a more permissive context for evolution of a unique holo-driven mechanism for kinetic control. Other soluble autoinhibition-based cyclic nucleotide receptors like EPAC or cGMP-dependent protein kinase do have the catalytic and cyclic nucleotide-regulatory regions fused, retaining the possibility of an additional holo-driven mechanism yet to be found.

Materials and Methods

Chimera C-2 is synonymous with the previously studied "HCN242 K381E" (16); other chimeras were assembled by PCR mutagenesis and verified by dideoxy sequencing. All derivatives contain identical non-CSD sequence of residues M1-G130 from mouse HCN2 (32) fused to M214-D521 of mouse HCN4 (16) with mutation K381E. This invariant sequence was fused to CSD sequence specific to each chimera: for C-del, a stop codon (mutation S522stop by HCN4 numbering); for C-1, S401-Q592 from mouse HCN1 (33) followed by three residues, LKA, due to a PCR artifact; for C-2, S444-H645 from mouse HCN2; for C-4, S522-H723 from mouse HCN4 with an E567G mutation due to a PCR artifact.

Channels were expressed as homomers in *Xenopus* oocytes obtained following guidelines of the Canadian Council on Animal Care and tested by patch clamp of inside-out excised membranes, all following previous procedures (16); recording conditions are briefly summarized here: solutions (in mM): extracellular, 5 NaCl, 92 KCl, 10 Hepes acid, 1 $MgCl_2$, 3$CaCl_2$, pH 7.4 with KOH; intracellular, same but 3 EGTA instead of $CaCl_2$, and Na-cAMP as needed. Currents were measured >3 min after patch excision when spontaneous changes in channel activity ("run-up") were observed to be complete. Kinetics were generally recorded with 20-kHz sampling and 10-kHz filtering, with subsequent digital 8-pole low-pass Bessel filtering at 1 kHz; Sylgard 184 (Dow) was used for kinetics with $\tau < 200$ ms (e.g., Fig. 3). For some recordings with $\tau > 500$ ms or steady-state measurements, sampling was 2 kHz; slow C-4 kinetics were simply filtered online at 1 kHz.

For *g*-V relationships in individual patches (Table S1 and Fig. 2*A*), conductance values (*g*) were fitted with the Boltzmann function, $g = A/\{1+\exp([V - V_{1/2}]/s)\} + g_{offset}$, where floating parameters were $V_{1/2}$ (midpoint activation voltage), *s* (reciprocal slope factor), A (maximal conductance), and g_{offset} (leak or instantaneous conductance). Summary *g*-V relationships (Figs. 1*C* and 2*B*) were compiled from multiple patches as described (16) using −140 mV as the standard voltage for normalization.

Deactivation time courses were fitted with equations using either three exponentials (after 50-ms activation at −215 mV in Fig. 3) or one exponential (after 2- or 3-s activation), with iterative fitting rounds as described in detail in ref. 16. This method defines a duration for the initial delay (*d*) corresponding to the concave-positive portion of the tail current (see Fig. 1*D* and Fig. S2).

Except where noted otherwise, results reported for holo channels were collected with 10 μM cAMP; this concentration was found to be saturating for all constructs (indistinguishable from 30 μM cAMP). Except where noted otherwise, numerical values reported are mean ± SD, n is the number of patches, and significance testing was by *t* test.

ACKNOWLEDGMENTS. We thank K. Magee for technical assistance, other Young lab members for discussions, and Drs. A. L. Zimmerman (Brown University, Providence, RI) and S. A. Siegelbaum (Columbia University, New York) for gifts of equipment and comments on the manuscript. Primary support: Discovery Grant from Natural Sciences and Engineering Research Council (NSERC) (to E.C.Y.). Other support: Scientist Development Grant from American Heart Association (to E.C.Y.) (for portions of work before 2007), Graduate Fellowships from Simon Fraser University and Brown University (to N.L.W.), and Postgraduate Scholarship from NSERC (to N.L.W.). E.C.Y. is a Scholar of the Michael Smith Foundation for Health Research.

1. Rehmann H, Wittinghofer A, Bos JL (2007) Capturing cyclic nucleotides in action: Snapshots from crystallographic studies. *Nat Rev Mol Cell Biol* 8:63–73.
2. Robinson RB, Siegelbaum SA (2003) Hyperpolarization-activated cation currents: From molecules to physiological function. *Annu Rev Physiol* 65:453–480.
3. Tse HF, et al. (2006) Bioartificial sinus node constructed via in vivo gene transfer of an engineered pacemaker HCN channel reduces the dependence on electronic pacemaker in a sick-sinus syndrome model. *Circulation* 114:1000–1011.
4. Murata Y, Iwasaki H, Sasaki M, Inaba K, Okamura Y (2005) Phosphoinositide phosphatase activity coupled to an intrinsic voltage sensor. *Nature* 435:1239–1243.
5. Männikkö R, Elinder F, Larsson HP (2002) Voltage-sensing mechanism is conserved among ion channels gated by opposite voltages. *Nature* 419:837–841.
6. Shin KS, Rothberg BS, Yellen G (2001) Blocker state dependence and trapping in hyperpolarization-activated cation channels: Evidence for an intracellular activation gate. *J Gen Physiol* 117:91–101.
7. Zagotta WN, et al. (2003) Structural basis for modulation and agonist specificity of HCN pacemaker channels. *Nature* 425:200–205.
8. Ulens C, Siegelbaum SA (2003) Regulation of hyperpolarization-activated HCN channels by cAMP through a gating switch in binding domain symmetry. *Neuron* 40:959–970.
9. DiFrancesco D, Tortora P (1991) Direct activation of cardiac pacemaker channels by intracellular cyclic AMP. *Nature* 351:145–147.

10. Barbuti A, Baruscotti M, Altomare C, Moroni A, DiFrancesco D (1999) Action of internal pronase on the f-channel kinetics in the rabbit SA node. *J Physiol* 520(Pt 3):737–744.
11. Wainger BJ, DeGennaro M, Santoro B, Siegelbaum SA, Tibbs GR (2001) Molecular mechanism of cAMP modulation of HCN pacemaker channels. *Nature* 411:805–810.
12. Pufall MA, Graves BJ (2002) Autoinhibitory domains: Modular effectors of cellular regulation. *Annu Rev Cell Dev Biol* 18:421–462.
13. Tao M, Salas ML, Lipmann F (1970) Mechanism of activation by adenosine 3′:5′-cyclic monophosphate of a protein phosphokinase from rabbit reticulocytes. *Proc Natl Acad Sci USA* 67:408–414.
14. de Rooij J, et al. (2000) Mechanism of regulation of the Epac family of cAMP-dependent RapGEFs. *J Biol Chem* 275:20829–20836.
15. Popovych N, Tzeng SR, Tonelli M, Ebright RH, Kalodimos CG (2009) Structural basis for cAMP-mediated allosteric control of the catabolite activator protein. *Proc Natl Acad Sci USA* 106:6927–6932.
16. Wicks NL, Chan KSC, Madden Z, Santoro B, Young EC (2009) Sensitivity of HCN channel deactivation to cAMP is amplified by an S4 mutation combined with activation mode shift. *Pflugers Arch* 458:877–889.
17. Tran N, et al. (2002) A conserved domain in the NH2 terminus important for assembly and functional expression of pacemaker channels. *J Biol Chem* 277:43588–43592.
18. Altomare C, et al. (2001) Integrated allosteric model of voltage gating of HCN channels. *J Gen Physiol* 117:519–532.
19. Wang J, Chen S, Siegelbaum SA (2001) Regulation of hyperpolarization-activated HCN channel gating and cAMP modulation due to interactions of COOH terminus and core transmembrane regions. *J Gen Physiol* 118:237–250.
20. Elinder F, Männikkö R, Pandey S, Larsson HP (2006) Mode shifts in the voltage gating of the mouse and human HCN2 and HCN4 channels. *J Physiol* 575:417–431.
21. Männikkö R, Pandey S, Larsson HP, Elinder F (2005) Hysteresis in the voltage dependence of HCN channels: Conversion between two modes affects pacemaker properties. *J Gen Physiol* 125:305–326.
22. Bruening-Wright A, Larsson HP (2007) Slow conformational changes of the voltage sensor during the mode shift in hyperpolarization-activated cyclic-nucleotide-gated channels. *J Neurosci* 27:270–278.
23. Bruening-Wright A, Elinder F, Larsson HP (2007) Kinetic relationship between the voltage sensor and the activation gate in spHCN channels. *J Gen Physiol* 130:71–81.
24. Chen S, Wang J, Zhou L, George MS, Siegelbaum SA (2007) Voltage sensor movement and cAMP binding allosterically regulate an inherently voltage-independent closed-open transition in HCN channels. *J Gen Physiol* 129:175–188.
25. Johnson JP, Jr, Zagotta WN (2005) The carboxyl-terminal region of cyclic nucleotide-modulated channels is a gating ring, not a permeation path. *Proc Natl Acad Sci USA* 102:2742–2747.
26. Craven KB, Olivier NB, Zagotta WN (2008) C-terminal movement during gating in cyclic nucleotide-modulated channels. *J Biol Chem* 283:14728–14738.
27. Prole DL, Yellen G (2006) Reversal of HCN channel voltage dependence via bridging of the S4-S5 linker and Post-S6. *J Gen Physiol* 128:273–282.
28. Kusch J, et al. (2010) Interdependence of receptor activation and ligand binding in HCN2 pacemaker channels. *Neuron* 67:75–85.
29. Scott SP, Shea PW, Dryer SE (2007) Mapping ligand interactions with the hyperpolarization activated cyclic nucleotide modulated (HCN) ion channel binding domain using a soluble construct. *Biochemistry* 46:9417–9431.
30. Kornev AP, Taylor SS, Ten Eyck LF (2008) A generalized allosteric mechanism for cis-regulated cyclic nucleotide binding domains. *PLoS Comput Biol* 4:e1000056.
31. Budde T, et al. (2005) Impaired regulation of thalamic pacemaker channels through an imbalance of subunit expression in absence epilepsy. *J Neurosci* 25:9871–9882.
32. Santoro B, et al. (2000) Molecular and functional heterogeneity of hyperpolarization-activated pacemaker channels in the mouse CNS. *J Neurosci* 20:5264–5275.
33. Santoro B, Grant SG, Bartsch D, Kandel ER (1997) Interactive cloning with the SH3 domain of N-src identifies a new brain specific ion channel protein, with homology to eag and cyclic nucleotide-gated channels. *Proc Natl Acad Sci USA* 94:14815–14820.